JOURNAL OF MATERIALS SCIENCE 26 (1991) 4361–4368

Cellular microstructure and heterogeneous coarsening of δ′ in rapidly solidified Al–Li–Ti alloys

M. LIEBLICH, M. TORRALBA
Centro Nacional de Investigaciones Metalúrgicas, CSIC, Avda. Gregorio del Amo 8, 28040 Madrid, Spain

Four melt-spun Al–Li–Ti alloys with ~2 wt% lithium and 0.10 to 0.35 wt% titanium have been obtained and heat-treated at 473 K for up to 1000 h. Rapid solidification gives rise to a matrix with titanium in solid solution which drastically alters the δ′ coarsening rate. While TEM studies of samples aged for short times show a homogeneous distribution of metastable δ′ phase, as ageing time is increased, and depending on the ribbon section, three different microstructures can be distinguished: (i) on the wheel side, the δ′ distribution is homogeneous; (ii) intermediate regions show δ′ particles delineating cells with narrow walls; (iii) on the gas side, δ′ particles delineate "circular" cells. A higher titanium content in the cell centres than on cell walls has been determined. The coarsening rate of δ′ in microstructure (i) above is slower than in binary Al–Li alloys. Cellular microstructures (ii) and (iii) show the preferential coarsening of δ′ particles on the walls, which is faster the higher the titanium concentration. Taking into account the fact that the partition coefficient of titanium in aluminium in the peritectic region is > 1, an explanation of δ′ phase evolution is given which leads to the conclusion that the effect of titanium in solid solution is to retain vacancies, restricting lithium diffusion.

1. Introduction

The interest of Al–Li alloys to the aerospace industry is due to their high Young's modulus and strength, combined with a low density [1]. Whereas Young's modulus and density are independent of whether lithium atoms are in solid solution or forming the ordered metastable δ′(Al_3Li) phase, the strength depends directly on the volume fraction of the metastable phase. The strengthening δ′ precipitates have an $L1_2$ superlattice structure, a spherical shape, and a cube–cube orientation relationship with the aluminium matrix. When an Al–Li alloy containing more than about 1 wt % lithium is quenched from the solid-solution field and aged at a temperature below the solvus line of δ′, homogeneous precipitation of the metastable phase occurs. Coarsening of δ′ depends on ageing time and temperature. Tamura *et al.* [2] first showed that at a given temperature the δ′ particle mean radius increases as $t^{1/3}$. With increasing ageing temperature the coarsening rate becomes higher.

Titanium is commonly used as grain refiner in aluminium alloys [3]. Moreover, it has a low solid solubility and diffusion rate in aluminium [4]; hence, with a low titanium addition, it is possible to obtain a high volume fraction of thermally stable precipitates. To avoid the presence of large intermetallic particles, rapid solidification techniques can be used. It has been reported [5] that at the peritectic temperature (938 K) titanium solid solubility increases up to 3.5 wt %.

By rapid solidification [6], undercooling of the melt and a high velocity of the solidification front are obtained, and these affect the nucleation processes to produce small grain and precipitate sizes. Apart from grain refining and extension of solid solubility, rapid solidification can give rise to other microstructural changes, such as precipitation of new metastable phases.

The metastable Al_3Ti phase has been found by several authors who carried out work on rapidly solidified Al–Li–Ti alloys with up to 1 wt % titanium [7–10]. This would agree with the prediction of Hori *et al.* [11] for binary Al–Ti alloys. According to these authors, the crystalline structure of Al_3Ti particles in binary Al–Ti alloys depends on the titanium content and solidification rate, changing from an ordered metastable $L1_2$ structure, at high solidification velocity and low titanium content, to stable $D0_{22}$-type Al_3Ti precipitates (Fig. 1).

Research on Al–Li–Ti alloys also shows the presence of a complex phase consisting of an $Al_3(Li_x, Ti_{1-x})$ core surrounded by δ′ phase. The $Al_3(Li_x, Ti_{1-x})$ particles would act as nuclei for δ′ and would be similar to the $Al_3(Li_x, Zr_{1-x})$ and $Al_3(Li_x, Hf_{1-x})$ phases found in Al–Li–Zr and Al–Li–Hf alloys [9, 10, 12].

In the present work the effect of titanium on the evolution of δ′ is studied in several melt-spun Al–Li–Ti alloys heat-treated at 473 K for up to 1000 h. Rapid solidification produces a matrix with titanium in solid solution, which drastically changes the δ′ coarsening rate [13]. Different microstructures have been systematically observed, and the results are related to the effect of rapid solidification on the ribbon

0022–2461/91 $03.00 + .12

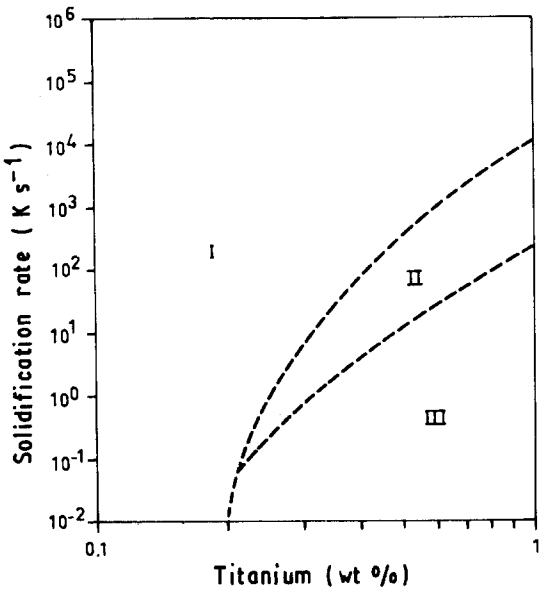

Figure 1 Interrelation between titanium content, solidification rate and solidification microstructure of Al–Ti alloys, from Hori *et al.* [11]. (I) Al(α) solid solution; (II) Al(α) + metastable $L1_2$-type Al_3Ti: (III) Al(α) + equilibrium $D0_{22}$-type Al_3Ti.

microstructure and to the effect of titanium in solid solution, which has a partition coefficient $k > 1$.

2. Experimental procedure

Four alloys were cast from Al–Li and Al–Ti alloys and from pure aluminium. They were subsequently melted in a fused silica tube and projected on a 0.28 m diameter beryllium–copper wheel rotating at a linear speed of $\sim 40\ m\ s^{-1}$ under a helium atmosphere. The compositions of the Al–Li–Ti melt-spun ribbons are listed in Table I.

Heat treatments were carried out for periods of up to 1000 h at 473 K in argon-filled glass capsules. Microstructures of the as-quenched and aged ribbons were characterized with scanning (SEM) and transmission (TEM) electron microscopes with energy-dispersive microanalysis units (EDS). SEM samples were etched in a 33% HNO_3–67% methanol ultrasonic bath. TEM foils were double-jet electro-thinned in a 33% HNO_3–67% methanol electrolyte at 243 K, and thoroughly cleaned with methanol in an ultrasonic bath.

TABLE I Composition of the Al–Li–Ti alloys

Alloy	Concentrations in wt % (at %)		
	Lithium	Titanium	Aluminium
A	1.88 (6.92)	0.35 (0.18)	Balance
B	2.33 (8.48)	0.20 (0.10)	Balance
C	2.26 (8.29)	0.15 (0.08)	Balance
D	2.02 (7.47)	0.10 (0.05)	Balance

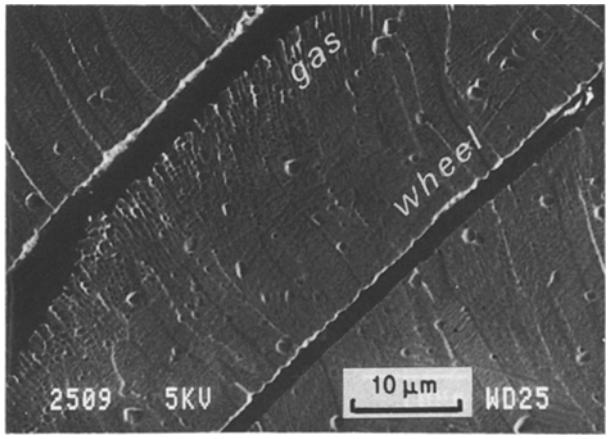

Figure 2 SEM micrograph of a longitudinal section. As-quenched alloy C (Al–2.26% Li–0.15% Ti).

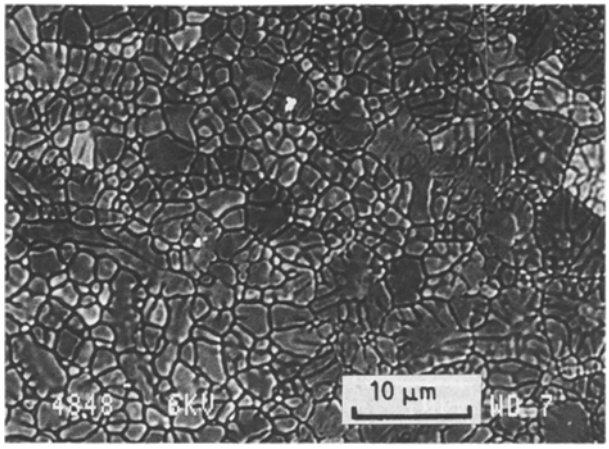

Figure 3 SEM micrograph of gas-side structure. As-quenched alloy A (Al–1.88% Li–0.35% Ti).

3. Results

3.1. As-quenched alloys

The melt-spun ribbons are 2 mm wide and 20–60 µm thick. On the wheel side, equiaxed grains with a 3 µm mean diameter are observed. The longitudinal sections (Fig. 2) show that solidification started on the wheel side, producing columnar grains of about 3 µm in width. Grains grow towards the gas side until the solid–liquid front rate decreases, giving rise to a cellular structure. Fig. 3, corresponding to the gas side of alloy A, shows the cellular structure which consists of grains of about 3 µm diameter formed by cells of < 1 µm diameter. EDS analyses of the SEM samples show heterogeneities in titanium distribution. As is shown in Fig. 4, the titanium content is always higher within the cells than on the walls. In the as-quenched condition the cell structure has not been detected by TEM.

The metastable δ′ phase has been detected in the as-quenched alloys through δ′ superlattice reflections in the electron diffraction patterns. This is in agreement with previous results on Al–Li alloys indicating that nucleation of δ′ takes place during solidification [14]. Dark-field images obtained with superlattice spots are too weak to show δ′ precipitates in the as-quenched condition. However, due to the low interfacial energy of the metastable phase, a homogeneous

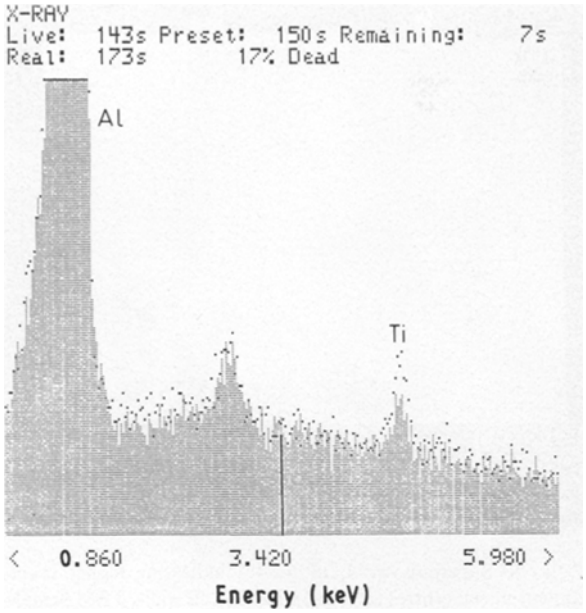

Figure 4 Superimposed EDS spectra indicating higher titanium content in cell centres (dots) than in cell walls (shaded). SEM sample of as-quenched alloy A (Al–1.88% Li–0.35% Ti).

distribution of fine δ′ nuclei throughout the matrix is expected.

No titanium-containing precipitates have been detected. Rapid solidification has given rise to a supersaturated solid solution of titanium in the aluminium matrix, which is in agreement with the predictions of Hori *et al.* [11]. Although the superlattice patterns might correspond to fine metastable $L1_2$-type Al_3Ti particles, there is no doubt that their origin is the δ′ phase, as will be discussed later.

3.2. Heat-treated alloys

For short ageing times at 473 K, dark-field images always show a homogeneous distribution of fine δ′ particles throughout the aluminium matrix, as shown in Fig. 5.

When the ageing time increases, a preferential coarsening of some δ′ particles delineating a cellular structure is observed in some grains. Depending on the ribbon section three different microstructures can be distinguished:

(i) On the wheel side, δ′ distribution remains homogeneous (Fig. 6).

(ii) The intermediate regions show a distribution of δ′ particles forming narrow-walled cells, the wall widths being about 50–100 nm. The microstructure consists mostly of equiaxed cells with a 0.5 μm mean diameter (Fig. 7), but sometimes elongated cells of 0.3–0.5 μm width can be seen, as shown in Fig. 8.

(iii) On the gas side, δ′ particles are distributed delineating "circular" cells of different sizes, with walls up to 0.8 μm in width, as shown in Fig. 9.

EDS analyses of microstructures (ii) and (iii) studied by TEM always indicate a higher titanium content in cell centres than on cell walls (Fig. 10). Therefore, cells observed by TEM can be related to those observed by SEM in the as-quenched alloys (Figs 2–4).

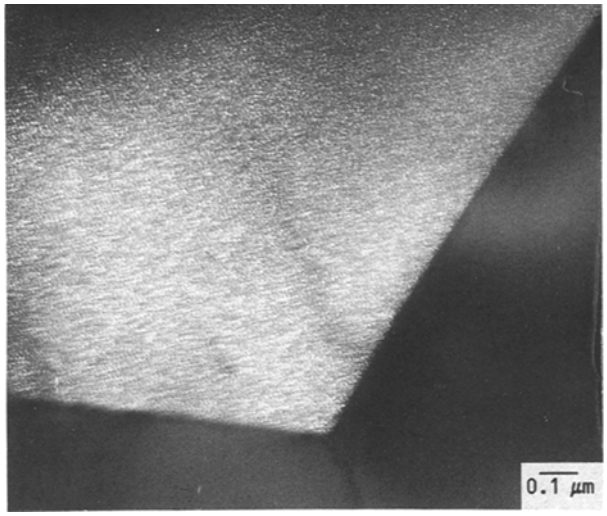

Figure 5 Dark-field image of the homogeneous distribution of δ′. Alloy B (Al–2.33% Li–0.20% Ti) aged at 473 K for 0.5 h.

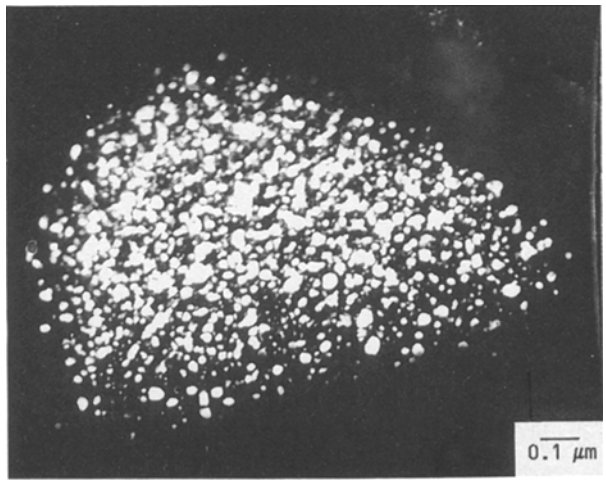

Figure 6 Dark-field image of the homogeneous distribution of δ′ on the wheel side. Alloy B (Al–2.33% Li–0.20% Ti) aged at 473 K for 500 h.

For a given temperature, the evolution of δ′ phase in an Al–Li alloy depends on the ageing time [2]. In the melt-spun Al–Li–Ti alloys, the coarsening and distribution of δ′ also depend on microstructure, i.e. ribbon section, and on titanium content.

3.2.1. Influence of microstructure

In microstructure (i), on the wheel side, coarsening of δ′ particles is similar to that in binary Al–Li alloys, the only difference being a smaller δ′ mean diameter [15, 16].

In the intermediate regions and on the gas side, giving microstructures (ii) and (iii), the homogeneous distribution observed for short ageing times changes to a cellular distribution. Cells with narrow walls can be seen after 1 h heat treatment in alloy A and after 6–12 h in alloys B, C and D. "Circular" cells first appear at about 6 h in alloy A and at about 12 h in alloys B, C and D. When the ageing time is not very long, due to the small δ′ particle size it is difficult to determine whether the cell walls have a greater number of δ′ particles, or larger particles, than within the

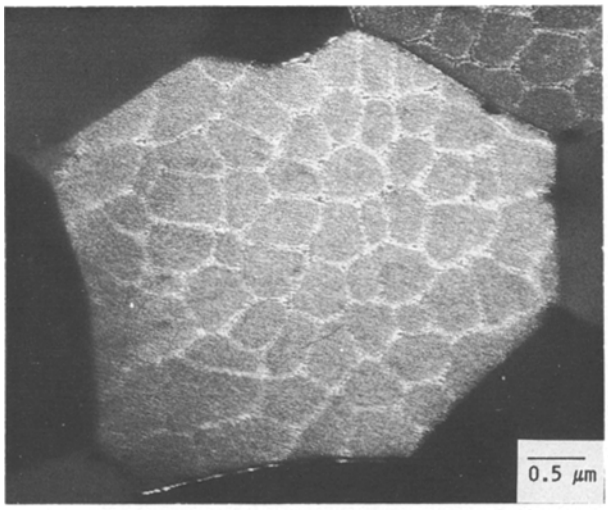

Figure 7 Dark-field image of δ′ particles delineating equiaxed cells of narrow walls in intermediate regions. Alloy A (Al–1.88% Li–0.35% Ti) aged at 473 K for 1 h.

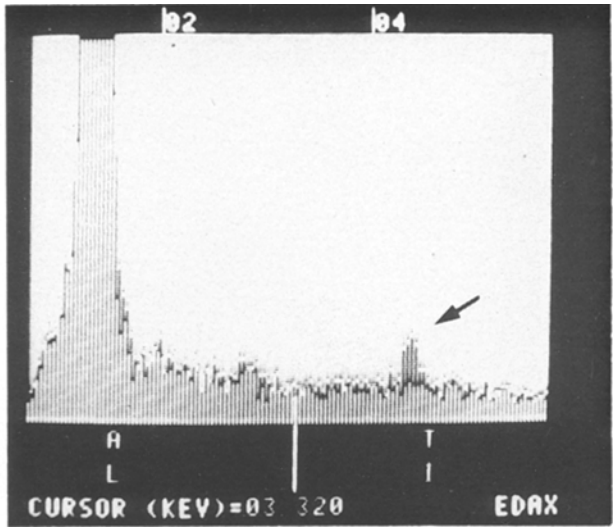

Figure 10 Superimposed EDS spectra indicating higher titanium content in cell centres (arrowed) than in cell walls. TEM sample of alloy A (Al–1.88% Li–0.35% Ti) aged at 473 K for 100 h.

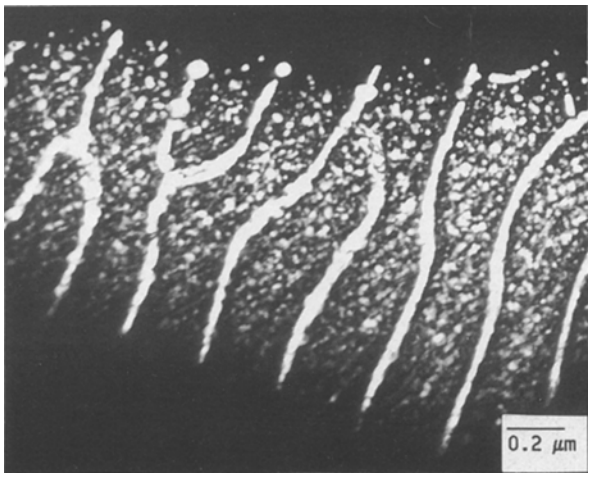

Figure 8 Dark-field image of δ′ particles delineating elongated cells of narrow walls in intermediate regions. Alloy C (Al–2.26% Li–0.15% Ti) aged at 473 K for 1000 h. Note coalescence of δ′ particles on the walls.

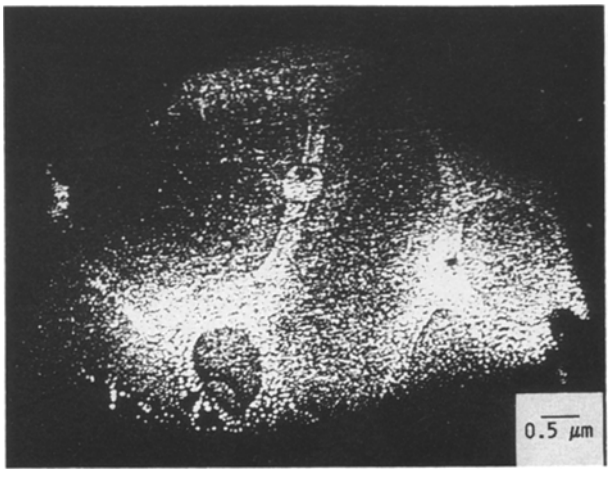

Figure 9 Dark-field image of δ′ particles delineating "circular" cells on the gas side. Alloy D (Al–2.02% Li–0.10% Ti) aged at 473 K for 100 h.

cells (see for example Fig. 7). As the ageing time is increased, the total number of δ′ precipitates decreases and cell evolution is such that δ′ particles on the walls coarsen, whilst δ′ particles within the cells hardly increase, or even diminish, in size. A decreasing δ′ volume fraction within the cells contributes to the coarsening of the precipitates on the walls. Fig. 11 shows dark-field images of alloy B aged for 48 and 500 h. While on average the precipitates on cell walls are larger at 500 h than at 48 h, precipitates within the cells coarsen only slightly. Moreover, in alloy A, which has the highest titanium content, after 500 h of heat treatment cells with δ′ particles only on cell walls can be found (Fig. 12).

Another feature of the evolution of the cellular microstructures of the melt-spun Al–Li–Ti alloys is that on cell walls, coarsening of δ′ particles induces the coalescence of some of them which then lose their spherical shape, as shown in Fig. 8. It is noteworthy that coalescence often occurs in these alloys, but only rarely in binary Al–Li alloys [17].

3.2.2. Influence of titanium on δ′ evolution

In microstructure (i) it was not possible to relate coarsening rate to titanium or lithium content due to the dispersion of the data. On the other hand, the evolution of the cellular microstructures is faster the higher the titanium content. Both microstructures (ii) and (iii) appear first in alloy A, which has the highest titanium content, where δ′ particles need only 1 h of heat treatment at 473 K in order to delineate the narrow-walled cells and 6 h to delineate the "circular" cells. Alloy A also presents the largest size difference between δ′ particles on walls and cell centres, as is confirmed by comparing, for example, microstructures of this alloy and alloy D. In alloy A (Fig. 13), at only 12 h of heat treatment, particles on the cell walls are much larger than particles within the cells. The behaviour of alloy D, with the lowest titanium content, has more in common with that of binary Al–Li alloys, and,

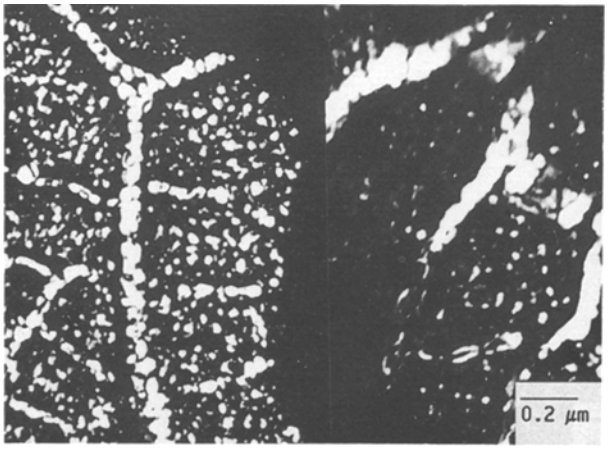

Figure 11 Dark-field image of alloy B (Al–2.33% Li–0.20% Ti) aged at 473 K for 48 h (left) and 500 h (right).

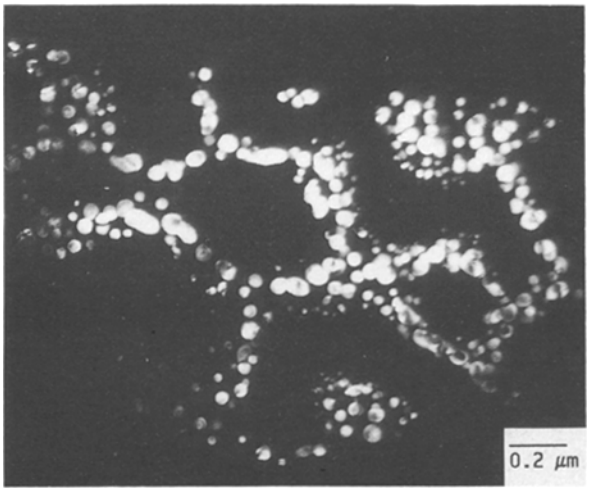

Figure 12 Dark-field image showing δ′ particles only on cell walls. Alloy A (Al–1.88% Li–0.35% Ti) aged at 473 K for 500 h.

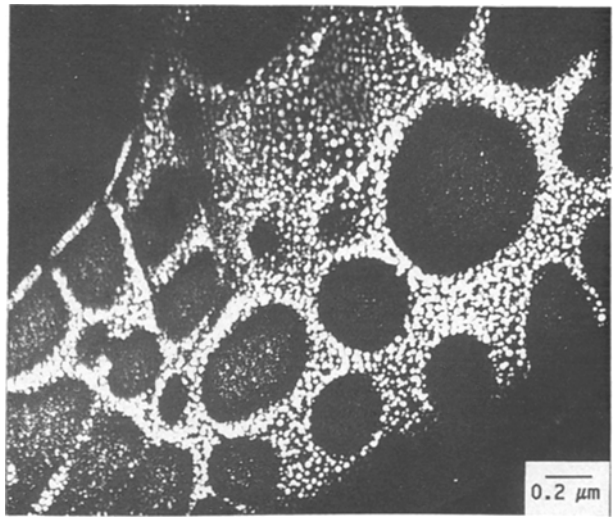

Figure 13 Dark-field image of alloy A (Al–1.88% Li–0.35% Ti) aged at 473 K for 12 h.

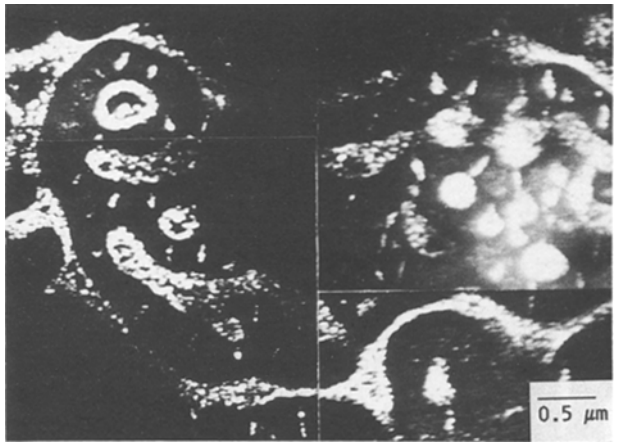

Figure 14 Dark-field image of alloy A (Al–1.88% Li–0.35% Ti) aged at 473 K for 12 h showing a grain with discontinuous cell walls due to the dissolution of some of their δ′ particles.

at 100 h of heat treatment (Fig. 9), differences between δ′ size within the cells and on the walls are still negligible. Figs 9 and 13 show a microstructure of "circular" cells, but similar differences appear in the microstructure of narrow-walled cells.

As evolution progresses, the dissolution of δ′ on the walls, and the precipitation of the stable δ(AlLi) phase on grain boundaries, take place. Once more, alloy A is the first one in which the walls start to fade due to the dissolution of their δ′ particles (Fig. 14).

4. Discussion

4.1. Origin of the cells

The cellular structure observed in the as-quenched alloys (Figs 2 and 3) is characteristic of the solidification method. It takes place in many rapidly solidified alloys and has been mentioned by several researchers [18, 19].

In the first stage of melt-spinning the solidification front velocity is very high, the solid–liquid interface is stable and a partitionless solidification takes place [20]. Once solidification starts, the temperature increases due to recalescence, which decreases liquid undercooling and, therefore, solidification front velocity. In that condition, any perturbation in the front immediately progresses giving rise to a cellular microstructure. To study the cell formation, classic undercooling theory [21, 22] is commonly used as a good approximation [19].

No information is available in the literature about the ternary Al–Li–Ti phase diagram and, therefore, the study of cell formation during rapid solidification was carried out considering the Al–Li and Al–Ti binary phase diagrams separately. As the titanium content is very low, this assumption can be considered accurate.

4.1.1. Al–Li system

In the current study, alloys are placed in the hypoeutectic region of the Al–Li system [23]. According to the constitutional undercooling theory, lithium concentration in the liquid at the solidification front is higher than the nominal concentration of lithium in the alloy, as shown in Fig. 15, where C_0(Li) is the nominal concentration of lithium and k(Li) ≈ 0.66 [4] is the partition coefficient of lithium in aluminium. Due to rapid solidification, a very high temperature gradient builds up in the liquid, and in the area

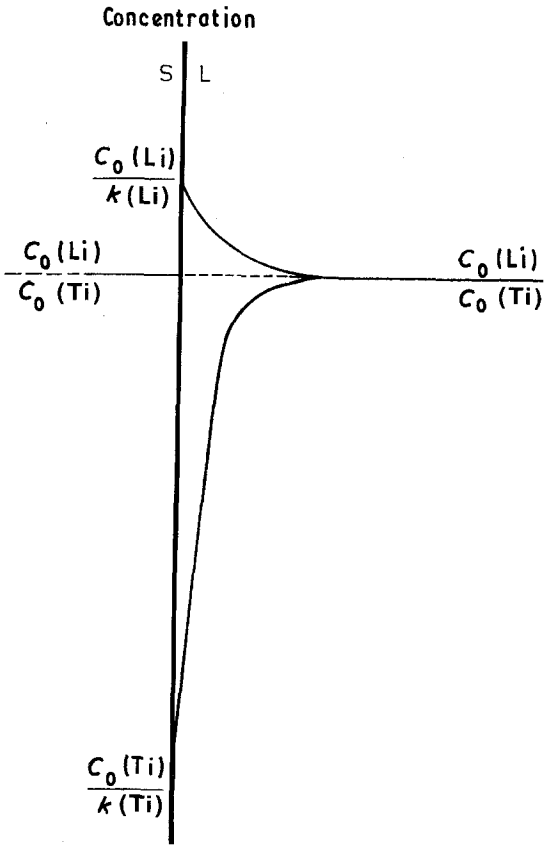

Figure 15 Lithium and titanium concentration profiles ahead of the solidification front.

ahead of the solidification front the liquid is highly constitutionally undercooled. Instabilities of the interface will give rise to the formation of cells. Cell tips, further within the liquid, will solidify with a lower lithium concentration than cell walls [24]. The final result will be a cellular microstructure with a lithium gradient.

4.1.2. Al–Ti system

In each cell, titanium atoms produce a similar effect superimposed on that of the lithium gradient. In this case, the Al–Ti system presents a peritectic reaction at the aluminium-rich side. Furthermore, for a very high solidification rate, the Al–Ti phase diagram can be assumed to be as shown in Fig. 16, where the liquidus and solidus lines have been extended [25]. For a peritectic, the solute concentration in the liquid at the solidification front is lower than the solute concentration of the alloy (Fig. 15). This is due to the partition coefficient, which is greater than unity for peritectics and has a value of $k(\mathrm{Ti}) \approx 10$ for titanium in aluminium [4]. As in the previous case, a very high temperature gradient is acting in the liquid. Any perturbation of the interface will give rise to the immediate formation of cells. In this case, cell tips, further within the liquid, will find a higher titanium content than cell walls [26].

4.1.3. Al–Li–Ti system

The sign and magnitude of solute gradients depend basically on the partition coefficients. Fig. 17 shows

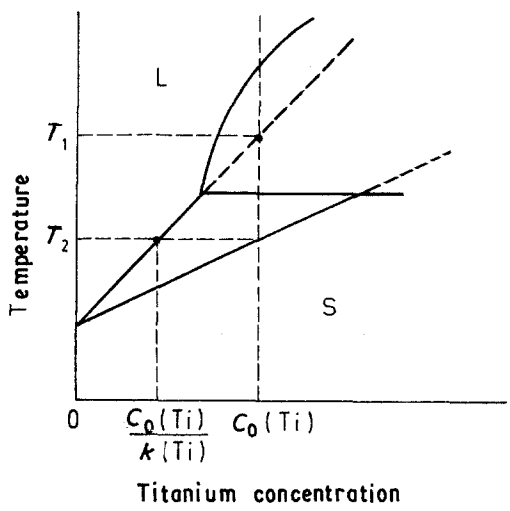

Figure 16 Al-rich side of the Al–Ti phase diagram.

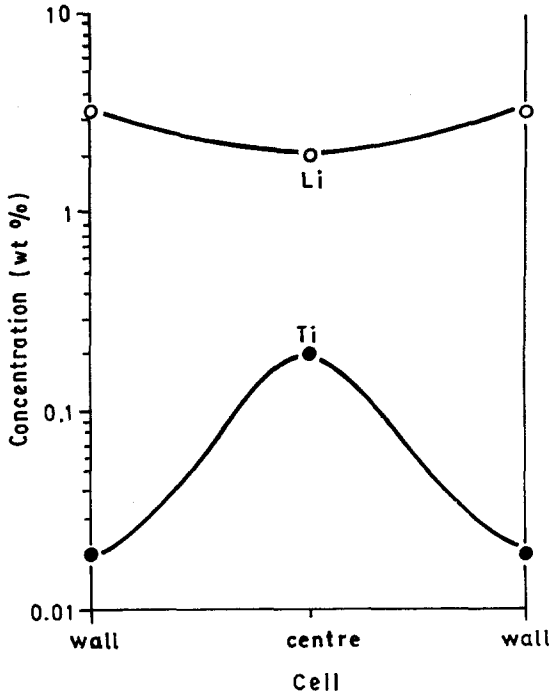

Figure 17 Lithium and titanium concentration profiles across a solidification cell.

schematically the concentration profiles of lithium and titanium across a cell, plotted in a logarithmic scale in order to compare the relative concentration differences. As can be seen, the lithium concentration is lower in the cell centre than on the wall, whereas the titanium concentration is higher in the cell centre than on the wall. On the other hand, the titanium gradient is much sharper than the lithium gradient.

The titanium gradient, which appears as a theoretical result, has been found experimentally in the as-quenched Al–Li–Ti ribbons (Fig. 4). The lithium distribution should be heterogeneous as well. Unfortunately, this fact was not verified by experimental measurements due to limitations of the EDS units to detect light elements.

Depending on the ribbon section, three different microstructures can be found in the as-quenched Al–Li–Ti alloys. Fig. 18 represents the solidification

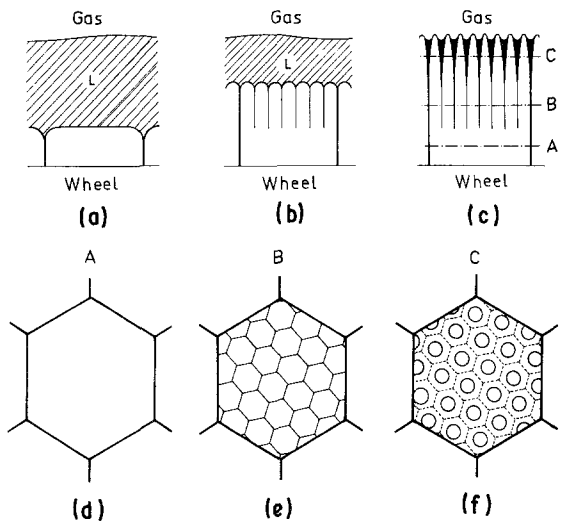

Figure 18 (a, b, c) Solidification process of a melt-spun ribbon; (d, e, f) grains corresponding to sections A, B and C of (c).

process of a melt-spun ribbon in three schematic stages. In the first one (Fig. 18a), the melt in contact with the wheel is abruptly undercooled, giving rise to a plane solid–liquid interface and to a homogeneous solute distribution throughout the grains. Therefore, on the wheel side (Fig. 18d), the structure will consist of grains with a uniform distribution of solute atoms.

As solidification progresses (Fig. 18b), latent heat increases the liquid temperature and, thus, the solidification front moves more slowly. At this stage any perturbation is stable and a cellular structure is formed. Within each cell, according to the classic undercooling theory extrapolated to high solidification rate, a heterogeneous distribution of solute atoms is created. Therefore, intermediate regions (Fig. 18e) will show a microstructure of equiaxed cells with narrow walls and lithium and titanium concentration gradients.

The microstructure of elongated cells with narrow walls would correspond to intermediate regions as well, probably to sections not perfectly perpendicular to the solidification direction. Apart from that, it could come from columnar grains which changed growth direction during solidification.

At the third stage (Fig. 18c), the solidification velocity is even slower and there is a larger amount of intercellular liquid, which is enriched in lithium and titanium-depleted. Therefore, on gas side (Fig. 18f) solute atoms will be distributed delineating "circular" cells with wide walls.

4.2. Cellular distribution of δ′

In the previous section, lithium and titanium gradients have been theoretically established for the solidification cells of the as-quenched Al–Li–Ti melt-spun alloys.

Due to the low diffusivity of titanium in aluminium, heat treatments at 473 K will not affect its original distribution in the matrix significantly. In fact, at 473 K the diffusion coefficient of titanium takes the value of $D_{Ti} = 5.8 \times 10^{-23}\ m^2\ s^{-1}$ [4] which leads to an effective diffusion distance in one dimension of ~ 15 nm for 1000 h ageing time. This value is very low, and it is clear that the titanium distribution will remain practically unchanged during ageing at 473 K. In contrast, the effective diffusion distance of a lithium atom for the same ageing time is ~ 1500 nm, two orders of magnitude higher.

Some doubts might arise about whether a supersaturated solid solution of titanium has been obtained during quenching, or whether fine metastable $L1_2$-type Al_3Ti particles have been formed. Metastable Al_3Ti phase would give rise to the same diffraction pattern as δ′ phase [11] and it would be nearly impossible to distinguish between them. As the titanium content is higher within the cells than on the walls, titanium precipitates, if present, would be mostly within the cells. For long ageing times, cells with only δ′ particles on the walls can be found (see Fig. 12). As diffraction patterns from the interior of this type of cell only give rise to matrix spots, superlattice reflections observed in the as-quenched alloys must arise exclusively from δ′, confirming that a solid solution of titanium has been obtained.

The most relevant result obtained in the melt-spun Al–Li–Ti alloys is the influence of the solidification cells and their solute gradients on δ′ coarsening.

Heterogeneous coarsening of δ′ cannot be due to the lithium gradient. Otherwise, this phenomenon would have been detected in other Al–Li alloys. Although the lithium content in the as-quenched alloys is higher on cell walls than within the cells, ageing at 473 K immediately smooths the lithium gradient due to the high diffusivity of this element in aluminium [4].

Dismissing lithium gradient as the source of this phenomenon, the titanium gradient must be responsible for the preferential coarsening of δ′ on the walls at the expense of δ′ within the cells. Coarsening of the metastable phase is controlled by lithium diffusion, and this in turn controlled by vacancies. This implies that titanium reduces the mobility of either lithium atoms or vacancies, restricting δ′ coarsening within the cells. It does not seem possible that titanium would trap lithium, as precipitates would have been formed and detected. That leaves only one possibility: that the effect of titanium in solid solution in the aluminium matrix is to retain vacancies. This would support the results of Kimura and Hasiguti [27], who found the same effect for tin in aluminium, and of Sanders [28], who suggested that the effect of retention of vacancies could be extended to other trace elements such as silver.

For short ageing times, as δ′ nucleation and growth are independent of the quenched-in vacancies [14], the titanium gradient does not alter these processes and a homogeneous δ′ precipitation takes place (Fig. 5).

On the other hand, as a consequence of the titanium gradient, the amount of free vacancies available to lithium diffusion is lower within the cells than on the walls. Therefore, with increasing ageing time lithium tends to diffuse to the walls, making coarsening of δ′ particles within the cells difficult. According to the

Ostwald ripening theory [21], diffusion takes place from the smaller to the larger particles. Thus, once preferential coarsening starts, size differences increase. This process progresses more and more efficiently, giving rise to the cellular distribution of δ′ phase.

The wheel side of the ribbons (Fig. 18d), as no solute gradient is present, will always show a homogeneous δ′ distribution and coarsening, differing from binary Al–Li alloys only in a slower coarsening rate. On the other hand, according to Fig. 18e and f, in intermediate regions and on the gas side of the ribbons a heterogeneous coarsening, and thus a cellular distribution of δ′, will take place.

The dependence of the evolution on titanium content in the cellular microstructures can be explained in the same way. A higher titanium content implies a higher free vacancies gradient, and thus a more pronounced lithium diffusion to the cell walls. Therefore, the cellular distribution of δ′ phase first appears in the most concentrated alloy, where the size difference between particles on cell centres and on cell walls is also higher for the same ageing conditions.

5. Summary and conclusions

The high cooling rate achieved by melt-spinning (10^5–10^6 K s^{-1}) gives rise to Al–Li–Ti alloys with titanium in solid solution. Moreover, during solidification, and depending on the ribbon section, a cellular distribution of solute atoms takes place. According to the constitutional undercooling theory, and as deduced from the Al–Ti phase diagram, a higher titanium content within the cells than on the cell walls is detected. Due to the low diffusivity of titanium in aluminium, ageing at 473 K does not affect its original concentration gradient.

The behaviour of δ′ in the melt-spun Al–Li–Ti alloys greatly differs from that in other Al–Li alloys. TEM studies of samples aged for short times reveal a homogeneous distribution of the metastable phase. With increasing ageing time, on the wheel side of the ribbons the δ′ distribution remains homogeneous and the δ′ coarsening rate is slower than in binary Al–Li alloys. In intermediate regions and on the gas side of the ribbons a cellular distribution is observed, due to the preferential coarsening of δ′ particles on the walls at the expense of those within the cells. On the other hand, it is determined that the evolution is faster, the higher the titanium concentration.

Taking into account that a cellular distribution of δ′ phase has not been observed in other Al–Li alloys, and that no titanium-containing precipitates have been detected, the heterogeneous coarsening of δ′ phase is attributed to the presence of titanium in solid solution. Trace elements with a partition coefficient $k > 1$, like titanium in the present alloys, would retain vacancies and restrict lithium diffusion within the solidification cells. Therefore, the different microstructures observed in the melt-spun Al–Li–Ti alloys appear as a consequence of the retention of vacancies by titanium atoms, and of the cellular microstructure created during the rapid solidification.

Acknowledgements

The authors wish to thank Professor G. Champier (ENSM, Nancy) for the use of facilities to obtain the melt-spun ribbons and for his valuable comments. Financial support by CICYT (Project MAT88-0254) is gratefully acknowledged.

References

1. T. H. SANDERS Jr and E. A. STARKE Jr, in Proceedings of 5th International Aluminium-Lithium Conference, Williamsburg, March 1989, edited by T. H. Sanders Jr and E. A. Starke Jr (MCE Publications, Birmingham, 1989) p. 1.
2. M. TAMURA, T. MORI and T. NAKAMURA, *J. Jpn. Inst. Met.* **34** (1970) 919.
3. S. E. NAESS and O. BERG, *Z. Metallkde* **65** (1974) 599.
4. L. F. MONDOLFO, "Aluminium Alloys: Structure and Properties" (Butterworths, London, 1976) pp. 6, 27, 385.
5. H. JONES, *Aluminium* **54** (1978) 274.
6. L. E. COLLINS, *Canad. Metall. Q.* **25** (1986) 59.
7. H. M. FLOWER and P. J. GREGSON, *Mater. Sci. Tech.* **3** (1987) 81.
8. Z. DI, S. SAJI, W. FUJITANI and S. HORI, *Trans. Jpn. Inst. Met.* **28** (1987) 827.
9. F. W. GAYLE, N. F. LEVOY and J. B. VANDERSANDE, *J. Met.* **5** (1987) 33.
10. N. F. LEVOY and J. B. VANDERSANDE, *Metall. Trans. A* **20** (1989) 999.
11. S. HORI, H. TAI and Y. NARITA, in Proceedings of 5th International Conference on Rapidly Quenched Metals, Wurzburg, FRG, 1985, edited by S. Steeb and H. Warlimont (North-Holland, Amsterdam, 1985) p. 911.
12. P. L. MAKIN and B. RALPH, *J. Mater. Sci.* **19** (1984) 3835.
13. M. LIEBLICH, M. TORRALBA and G. CHAMPIER, *J. Physique* **48** (1987) 465.
14. B. NOBLE and G. E. THOMPSON, *Met. Sci. J.* **5** (1971) 114.
15. S. F. BAUMANN and D. B. WILLIAMS, *Scripta Metall.* **18** (1984) 611.
16. F. H. SAMUEL and G. CHAMPIER, *J. Mater. Sci.* **22** (1987) 3851.
17. K. MAHALINGAM, B. P. GU, G. L. LIEDL and T. H. SANDERS Jr, *Acta Metall.* **35** (1987) 483.
18. F. H. SAMUEL, *Metall. Trans. A* **17** (1986) 73.
19. J. M. SATER, S. C. JHA and T. H. SANDERS Jr, *Mater. Sci. Engng* **91** (1987) 201.
20. H. JONES, *ibid.* **65** (1984) 145.
21. R. W. CAHN and P. HAASEN, "Physical Metallurgy" (North-Holland Physics, Amsterdam, 1983).
22. R. ELLIOTT, "Eutectic Solidification Processing, Crystalline and Glassy Alloys" (Butterworths, London, 1983).
23. T. B. MASSALSKI, "Binary Alloy Phase Diagrams" (American Society for Metals, Ohio, 1986).
24. T. M. MACKEY and T. F. KELLY, *Acta Metall.* **36** (1988) 2587.
25. H. W. KERR, J. CISSE and G. F. BOLLING, *ibid.* **22** (1974) 677.
26. S. P. MIDSON and H. JONES, in Proceedings of 4th International Conference on Rapidly Quenched Metals, Sendai, 1981, edited by T. Masumoto and K. Suzuki (Japan Institute of Metals, Sendai, 1982) p. 1539.
27. H. KIMURA and R. R. HASIGUTI, *Acta Metall.* **9** (1961) 1076.
28. T. H. SANDERS Jr, "Precipitation Mechanisms in Aluminum-Lithium Alloys" (School of Materials Engineering, Purdue University, 1983).

Received 7 March
and accepted 3 December 1990